Pure Appl. Chem., Vol. 78, No. 10, pp. 1843–1855, 2006.
doi:10.1351/pac200678101843

Materials of cellulose derivatives and fiber-reinforced cellulose–polypropylene composites: Characterization and application*

Peter Zugenmaier

Institute of Physical Chemistry, Clausthal University of Technology, Arnold-Sommerfeld-Strasse 4, D-38678 Clausthal-Zellerfeld, Germany

Abstract: Cellulose is a biodegradable polymer produced sustainably in large quantities by nature. It has been used by mankind for centuries because of its favorable properties, but suffers disadvantages such as the high cost of production and limited processibility. For example, it cannot be melted and is only soluble in less common solvents. The latter limitation can be overcome through appropriate derivatization of cellulose, which increases the solubility range and may generate thermoplastic materials. This paper will review three new developments leading to enhanced utilization of cellulosics.

Firstly, an overview is given of the progress in the formulation of fiber-reinforced thermoplastic cellulose composites to facilitate extrusion processing. Cellulose–polypropylene composites show enhanced properties in comparison with neat polypropylene, and offer scope for replacing composites containing glass fibers, owing to resultant advantages in weight, recyclability, and ease of disposal. Progress is also reported in improving the predictability of essential physical quantities and melt flow in cellulose esters. Finally, an account is given of the successful development of microcrystalline cellulose (CFM) derivatives, synthesized in a heterogeneous manner, as chiral recognition agents in liquid chromatography. The structural features of these materials are decisive for their use. A model is proposed for the morphology of the cellulosic fibrils.

Keywords: cellulose–polypropylene composites; cellulose mixed esters; chiral recognition; model of cellulosic fibrils; DMTA; conformation and packing of cellulose tribenzoate.

INTRODUCTION

Cellulose represents a renewable, enantiomeric, and polymeric material with special properties as biocompatibility, biodegradation, and, in wood as a composite with lignin and hemicelluloses, long-term durable and extreme-resistant raw materials in a wide temperature range. Cellulose is produced by photosynthesis of an estimated 10^{11} t/a in land plants [1]. The resulting technical importance is underlined by the fact that about one-half of the industrial applied polymers rest on a cellulose basis [2]. Mainly wood and cotton serve as industrial resources for paper, cardboard, and the textile industry (165×10^6 t/a) as well as for purified cellulose (7×10^6 t/a) necessary for the production of viscose and acetate fibers, films, and cellulose derivatives [3]. Cellulose ethers and esters are important cellulose derivatives and are used for a variety of technical applications [4,5].

*Paper based on a presentation at the 15th International Symposium on Fine Chemistry and Functional Polymers (FCFP-XV) and the 1st International Symposium on Novel Materials and their Synthesis (NMS-I), 17–20 October 2005, Shanghai, China. Other presentations are published in this issue, pp. 1803–1896.

Cellulose (Fig. 1) can be regarded as a semi-flexible linear chain of 1-4-linked β-D-glucopyranose units with a high degree of polymerization (DP) in native fibers (up to 6×10^3–13×10^3 in cotton linters [6]), which is drastically lowered by processing the native fibers or wood pulp. Since cellulose possesses a reducing and a nonreducing end, a chain direction can be defined, and the chain arrangement in the native fiber (cellulose I) is described by parallel running chains and the arrangement of cellulose II by antiparallel packed chains. Chain folding commonly established in synthetic polymeric materials can be excluded in the discussed low DP of cellulose I and II structures, and fringed micellar fibrils have been established.

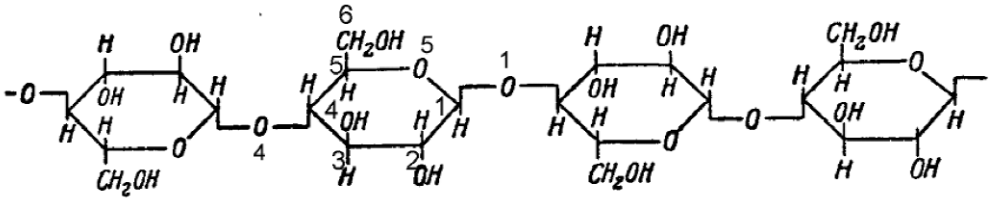

Fig. 1 Chemical constitution of cellulose as a linear chain of 1-4-linked β-D-glucopyranose units and numbering of carbon and oxygen atoms in the representation of Haworth (1932).

Considerable progress in application of polymeric materials has occurred by improved processing as well as by combining favorable properties of polymers in composites. The basic industrial requirements are simple and easy manufacture of the materials, melt processing at low cost, as well as the creation of tailored and durable materials.

In this review, we will address interesting topics of cellulosic research and application: Thermoplastic fiber-reinforced cellulose–polypropylene composites [7–13], predictions of some bulk properties for cellulose mixed esters as well as improvements for melt flow behavior [9,14] and some basic structural insights on materials applied in enantiomeric separation columns as stationary phase [15–20].

FIBER-REINFORCED CELLULOSE–POLYPROPYLENE COMPOSITES

Materials and methods

High-quality stiff cellulose fibers are of interest for reinforced composites. In recent years, investigation were carried out on thermoplastic fiber-reinforced cellulose commodity polymers for injection molding, wood-fiber plastic composites mainly for construction, and nanocomposites for high-performance composite materials. The new class of fiber-reinforced commodity composites will be reviewed, in which cellulose fibers of various types have been incorporated and thermoplastic matrices of low cost used as polypropylene or biodegradable materials as polylactide or cellulose acetate (CA) [21].

Isotactic polypropylene (PP, M_w = 263 10^3 g mol^{-1}) served as polymer matrix for the preparation of cellulose composites discussed below [7–10]. Two different types of cellulose materials were used as fillers: chopped strands of high-tenacity rayon filament yarn (viscose fibers, CFS) to a length of 8 mm and microcrystalline cellulose (CFM) from leave wood approximately 40 μm in length and 20 μm in cross-section. In addition, powdered xylan (hemi-cellulose, XL) from birch wood was also studied as filler. Xylan is a by-product of no use from the pulping process. In some of the investigations, maleic anhydride modified PP-homopolymer (MAPP) was added as compatibilizing agent.

A twin-screw extruder was used for mixing and homogenizing each filler type with the melted polymer matrix at a certain ratio. When necessary, a small amount (ca. 7 wt %) of the coupling agent MAPP was added. The samples for mechanical investigations were prepared by hot-pressing the extruded granules in a hydraulic, electrically heated press at 190 °C to about 0.3 mm in thickness and then

cooled to room temperature under pressure. Drawn samples were obtained by cutting stripes of ca. 6 mm width from the film and placed in a computer-controlled tensile testing device. The drawing process was carried out at a speed of 5 mm min^{-1} to various draw ratios (λ) and the samples immediately transferred to ice water.

The dynamic-mechanical thermo-analyzer (DMTA) served as main characterization method. Additional investigations have been carried out by thermal analysis (DSC) to determine melting and crystallization behavior, optical and electron microscopy for illustrating the contact between the components, X-ray investigations to check orientation and crystallinity. The conclusions obtained from these additional investigations support the DMTA analysis, but will not be discussed in detail here.

Stress-strain oscillations were performed with the DMTA instrument at a frequency of 10 Hz. The samples of the size 30×5 mm^2 area and 0.3 mm in thickness were placed in an insulated chamber, cooled down to ca –125 °C and then heated under a strain-controlled sinusoidal tensile loading to 170 °C with a heating rate of 2 °C min^{-1}. The viscoelastic properties, i.e., the complex dynamic modulus ($E^* = E'(\omega t) + i\, E''(\omega t)$; E" and E' loss and storage modulus, respectively) as well as the mechanical loss factor (damping) $\tan\delta = E''/E'$, were recorded as a function of temperature. The storage modulus E' describes the reversible stored energy, an important quantity for evaluating possible applications of the materials, and represents a measure of the stiffness of the materials. E' and especially E" or $\tan\delta$ are sensitive quantities for the uptake of energy changing the viscoelastic behavior of the sample. Especially, a peak in E" or $\tan\delta$ curves mirrors the onset of motions within the molecule or in the materials. The motions of whole segments of the polymer chains lead to a large peak in $\tan\delta$ and simultaneously to a significant drop in the stiffness of the materials and can be related to the glass transition of the materials. But motions of the side groups and compatibilizer added may also be detected in the DMTA spectra as smaller peaks of the E" or $\tan\delta$ curves. All relaxation peaks are usually denoted by Greek letters.

Results and discussion

The dynamic-mechanical spectra (storage modulus E' and damping factor $\tan\delta$) are shown for neat PP and compared to PP + 30 wt % filler (XL, CFM, CFS) in Fig. 2. Relaxation peaks are observed for the $\tan\delta$ curves in the vicinity of –80 °C (γ), 8 °C (β), and 100 °C (α), which are caused by the onset of the various motions of the chain molecules. The dominant β-peak represents the glass-to-rubber transition of the amorphous portion in PP and is assigned to the glass transition temperature. A significant decrease of the storage modulus E' is initiated at this transition. The curve drops even more drastically in the melting range of PP at about 150 °C.

The DMTA spectra of Fig. 2 show an increase of the storage modulus E' for the fiber-reinforced composites and a decrease of $\tan\delta$ as compared to neat PP with minor changes in the shapes of the curves. This observation can be interpreted as an increase in stiffness of the materials, highest for PP/CFS. The increase in stiffness is especially pronounced at higher temperatures below the melting temperature range. A better comparison of E' can be achieved for various kinds and amounts of fillers at a fixed temperature, e.g., at 20 °C (see Table 1). Data from previous work [22,23] with glass and polyester fibers as reinforcement agent have been added. It is interesting to note that the E' modulus for PP + 50 wt % CFM without adding any compatibilizer lies only 10 % below the value with the compatibilizer MAPP added. The storage modulus E' of composites with glass fibers can be reached with some higher CFS-filler content. XL as filler is not as effective as cellulose. It seems that the two heterogeneous parts, PP and cellulose, are in close contact through a hydrophobic interaction, which can be explained by consideration of the packing arrangement of the cellulose chains. The hydrophilic part of the cellulose chain is compensated by hydrogen bonds interconnecting the flat cellulose molecules edge on and thus forming sheets with hydrophobic surfaces. These sheets also cover to a large extent the surface of the cellulose crystallites and fibers and are responsible for the hydrophobic interaction with the polypropylene molecules.

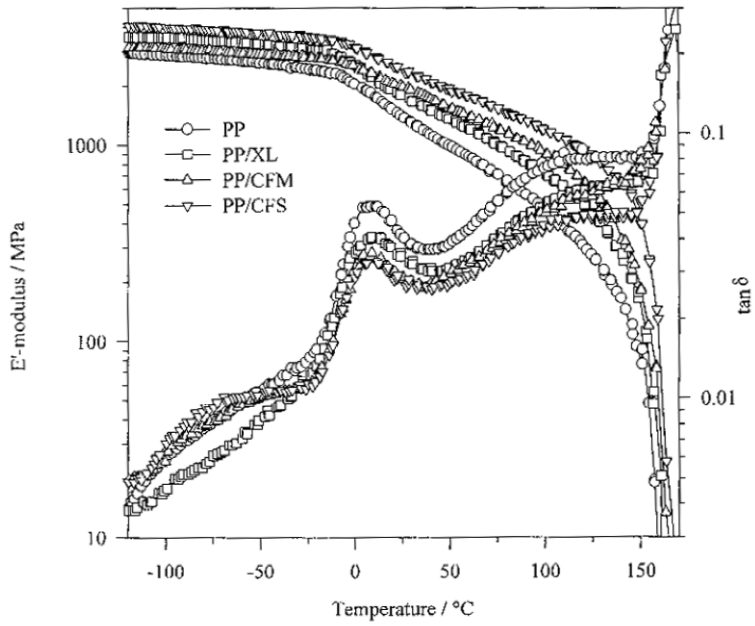

Fig. 2 DMTA spectra with storage modulus E' (upper curves) and damping factor tanδ (lower curves) as a function of temperature for neat PP and PP + 30 wt % filler content (XL: xylan filler, CFM: microcrystalline cellulose, CFS: high-tenacity rayon fiber).

Table 1 Storage modulus E' of isotropic samples.

Materials (matrix + wt % filler + MAPP)	E' [MPa] (at 20 °C)
Polypropylene–homopolymer (PP)	1560
PP + 20 % glass fibers (GF)	2700
PP + 20 % polyester fibers (PETF)	1840
PP + 20 % cellulose fibers (CFS, rayon)	2170
PP + 30 % cellulose fibers (CFS, rayon)	2725
PP + 30 % cellulose microcrystals (CFM)	2090
PP + 30 % xylan (XL)	1890
PP + 50 % CFM	2865
PP + 50 % CFM without MAPP	2585

A good adhesion between cellulose and polypropylene is also suggested by further observations. The crystallization temperature found by DSC experiments increases with higher amounts of cellulose filler and is caused by an easy nucleation at the surface of the cellulose fibers. This nucleation is visible by a widespread *trans*-crystallization morphology of PP occurring at the surface of the cellulose fibers and is illustrated in Fig. 3.

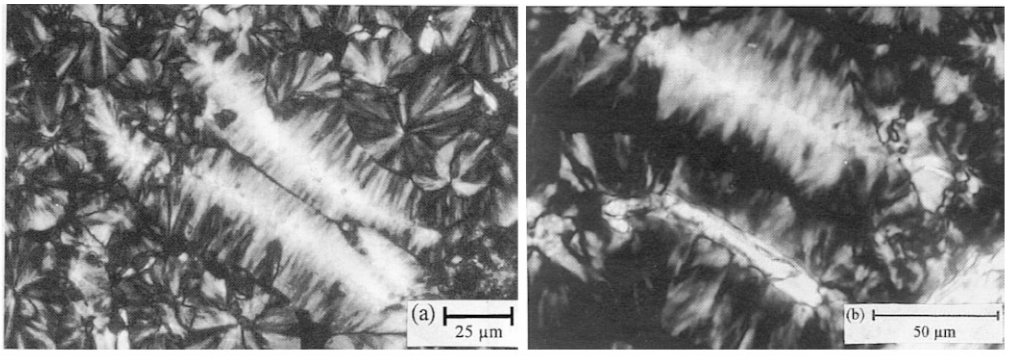

Fig. 3 Optical micrographs showing the *trans*-crystallization in selected samples of (a) PP + 30 wt % XL and (b) PP + 30 wt % CFM composites.

Figure 4 illustrates the DMTA spectra of drawn samples. According to fiber X-ray data, the anisotropic-oriented PP crystallites of neat PP and those from the composites are uniaxially oriented around the draw direction. Generally, it is observed that the storage modulus E' is increased with the draw ratio for all composites, including neat PP, and consequently the damping factor tanδ is decreasing with the draw ratio. The steep decrease of the E' curves at the melting range does not join in one melting temperature at very low E' values. The melting temperature of PP and the fiber-reinforced composites increases with the draw ratio and confirms the constraint melting under tension [24], which is higher than the equilibrium melting of isotropic materials and is also confirmed by DSC experiments. The melting temperature of the cellulose-PP composites exceeds the one of neat PP of the same draw ratio and suggests an increase of constraint melting caused by additional excellent contacts and adhesion between the two heterogeneous materials. From an application point of view, the increase of the storage modulus at higher temperature is remarkable for neat PP as well as for the composites as com-

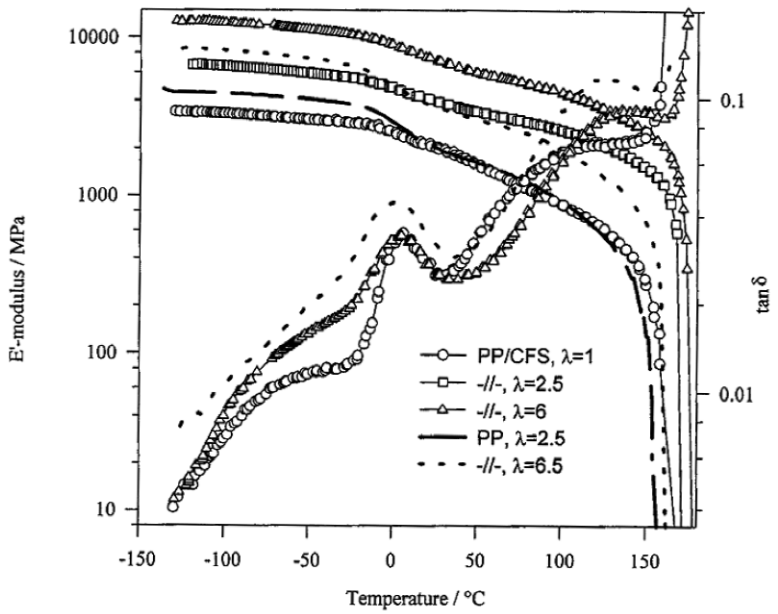

Fig. 4 DMTA spectra of neat PP and PP + 20 wt % CFS composites. The initial isotropic specimen PP/CFS (λ = 1) is compared with drawn ones of various draw ratios λ provided in the insert. E' in draw direction.

pared to the isotropic materials. For example, at 150 °C the storage modulus E' for PP + 20 wt % CFS amounts to 300 MPa for the isotropic sample ($\lambda = 1$) and for a draw ratio $\lambda = 6$ to 2600 MPa in contrast to neat PP with 30 MPa ($\lambda = 1$) and 650 MPa ($\lambda = 6.5$).

The basic thermal properties as melting and glass transition for fiber-reinforced composites are primarily influenced by the matrix materials and can be adjusted to the needs for special application by changing the matrix materials. The DMTA spectra of a so-called atactic polypropylene is shown in Fig. 5 obtained as a by-product in a suspension synthesis process of producing isotactic PP. Less stiffness is observed over the whole temperature range as compared to PP of Fig. 2 and to a mixture with PP (Fig. 5). It should be noted that some crystalline parts are still present in the APPS materials.

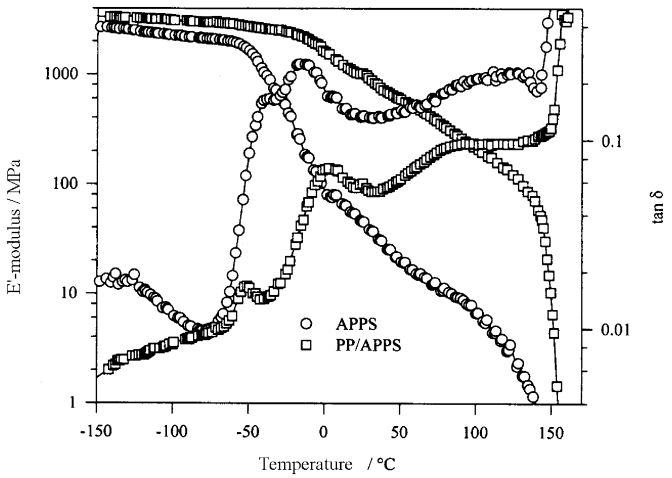

Fig. 5 DMTA spectra of a so-called APPS and a mixture of PP and APPS (PP/40 wt % APPS).

The viscoelastic behavior of the fiber-reinforced polypropylene–cellulose composites discussed is strongly influenced by the presence of cellulose fibers due to interfacial adhesion in contrast to the melting behavior. This outstanding adhesion is still present after melting the materials and reuse of a second time. Thermoplastic cellulose materials as fiber-reinforced composites of up to 50 wt % cellulose have been produced with excellent properties.

CELLULOSE-MIXED DERIVATIVES

Materials and methods

The difficulties in processing pure cellulose can be avoided, but nevertheless, the advantage of the stiff cellulose backbone preserved by derivatization to solvable and meltable compounds as, e.g., most cellulose esters.

The derivatization of cellulose to tri-substituted, partial substituted, or mixed substituted cellulose esters or carbamates was carried out in the system DMAc (*N*,*N*-dimethylacetamide)/LiCl as solvent. This solvent system is known to provide a random distribution of the side groups along the chain for partial substituted derivatives, and the original chain length is retained. Figure 6 represents the corresponding side groups applied for the compounds investigated [25]. However, the commercially available 2.5-substituted CA is widely used as starting compound to produce tri-substituted materials. In contrast to the polymers derivatized in the DMAc/LiCl system, CA exhibits a block-wise distribution of acetyl groups along the chain.

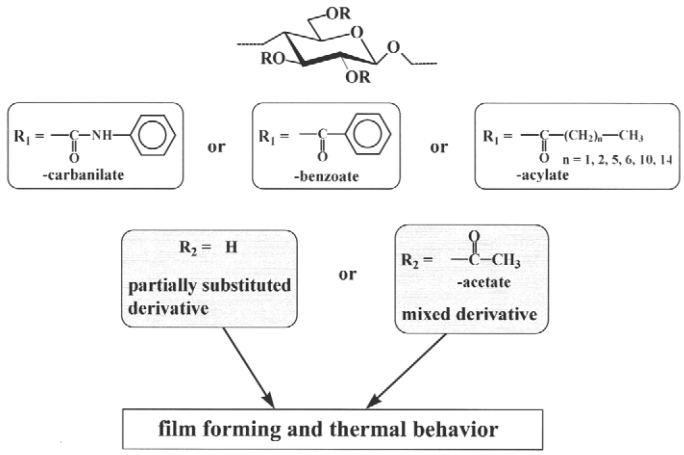

Fig. 6 Schematic representation of cellulose derivatives. R of the anhydroglucopyranose residue is substituted by R_1 for the tri-substitution and by R_1 and/or R_2 for partial or full substitution.

The DP, and the kind as well as the degree of substituents (DS) are varied for the derivatives synthesized. The storage modulus E' and the glass transition temperature T_g are determined by DMTA investigations as important physical properties for projected applications. The temperature of the peak of the damping curve is defined as T_g. The samples investigated are obtained by solvent evaporation, and sheets of 0.1 mm in thickness were produced. The sheets are cut to 30 mm in length, 4 mm in width for use in the DMTA equipment. They are dried for 24 h in vacuum at 80 °C and then cooled down to –150 °C to start the measurements with a heating rate of 1 K/min and a frequency of 10 Hz.

Results and discussion

Injection molding of cellulose esters, the main processing procedure for these materials, requires low melt flow. Improvement of melt flow can be obtained by fully substituting the already highly substituted compounds. DMTA measurements may serve to following this improvement. The storage modulus and the usable temperature range of low substituted cellulose acylates (DP = 200) from propionate to palmitate is predominately governed by the stiff cellulose backbone, and these materials exhibit a similar thermal behavior. If highly substituted (DS = 2.8) specimens are investigated as shown in Fig. 7, the breakdown of the stiffness of these materials (E') shifts to lower temperature values due to the plasticizer effect of the side groups and differentiates between the sizes of the side groups. A wide rubber plateau with still considerable storage modulus (equivalent to the melt viscosity) follows the steep drop of E' for small side groups, but E' drops to lower values for larger side groups. However, if the samples are peracetylated to fully substituted materials, the DMTA spectra of the right picture of Fig. 7 are obtained. The rubber plateau of the samples with smaller side groups are almost nonexistent, and the stiffness of the materials (melt viscosity) drops to very low values before degradation of the materials occurs at high temperatures. The melt flow reaches values that melt processing seems possible. Further, the choice of a side group regulates the temperature range for a desired application.

The prediction of tailored physical properties for specific application represents a further challenge for designing materials besides the excellent melt flow behavior discussed. The storage modulus E' and T_g rank high among these properties. A wide range of E' and T_g is observed for mixed cellulose derivatives. A table including all the data can be helpful, but plots of E' or T_g as a function of structural or interaction parameters, which correlate with the size of the various side groups, will ideally fulfill the selection of the data needed.

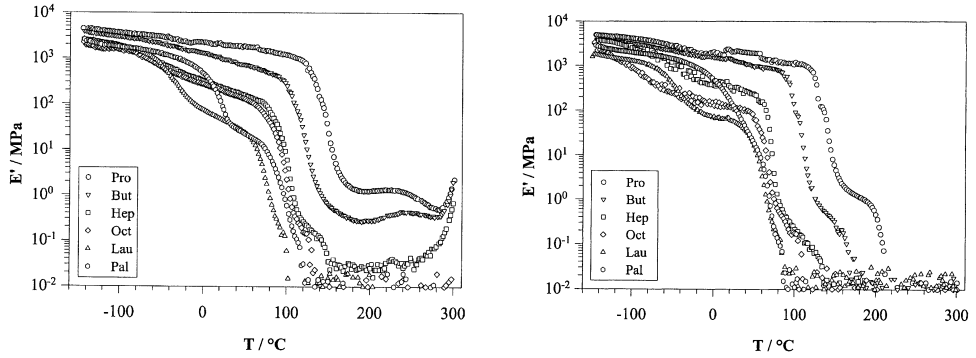

Fig. 7 DMTA spectra of highly substituted cellulose propionate, butyrate, heptanoate, octanoate, laurate, and palmitate (DS = 2.8, left) and the fully substituted specimens with the remaining OH groups of the samples of the left picture acetylated (right).

The side groups predominantly govern the interactions of cellulosic chains. An interaction parameter δ_L between polymers can be defined similar to the solubility parameters refined by Coleman et al. [26].

$$\delta_L = \Sigma\,(F_i/\Sigma\,V_{mi}) \tag{1}$$

where V_{mi} is the group molar volume and F_i the group molar attraction constant of the molar groups, i.e., $–CH_2–$ or –COO–. The needed values for F_i and V_{mi} are collected in [26]. Edgar et al. [27] found a linear relationship between δ_L, T_g, viscosity, and flexural modulus for CA as well as for various CA derivatives with a partial degree of substitution of 2.7 and completed to fully substituted compounds with ester groups from C_3 to C_7. Extending the database, the plots of Fig. 8 were obtained for the storage modulus E' at 25 °C (left) and T_g (right). A large number of CA derivatives, cellulose acylates, cellulose phenylcarbamates, and cellulose benzoates of various DP [14] as well as the published cellulose acylate-acetate data [27] have been considered in these plots.

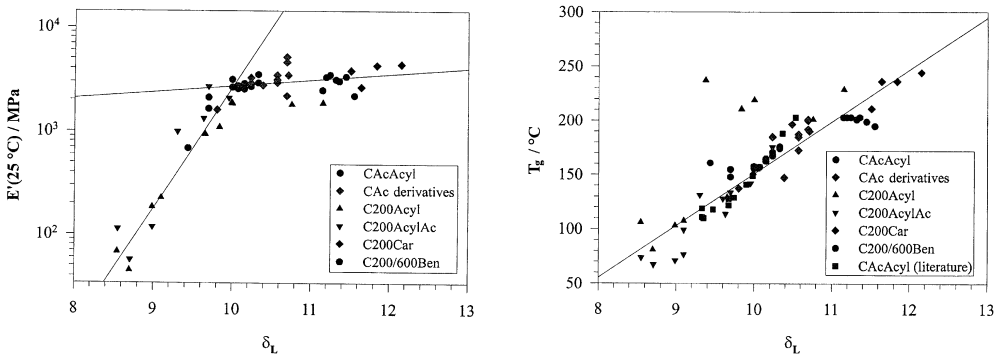

Fig. 8 Storage modulus E' at 25 °C (left) and T_g (right) of a large number of mixed CA derivatives and acylates, carbanilates, benzoates, as a function of the interaction parameter δ_L .

The calculated interaction parameter δ_L decreases monotonically with increasing DS and alkyl substituent length. Therefore, a perfect linear relationship of T_g with δ_L cannot be expected and is not obtained in the plot. Nevertheless, the straight line drawn in the plot is sufficient to reach acceptable T_g for arbitrary derivatives of which the interaction parameter can be easily calculated. It should also be noted that derivatives with longer side groups and DS = 1 exhibit significant deviations due to a two-

phase behavior caused by different stiffness of the main chain in comparison to the side groups as well as extensive hydrogen-bonding interactions.

The storage modulus E' at room temperature exhibits a two-range behavior in the plot of Fig. 8, which can be represented by two straight lines. Given a known interaction parameter δ_L, the storage modulus E' as well as T_g can be estimated or if a certain E' or T_g is desired, specific side groups can be proposed to fulfil the requirement.

ENANTIOMERIC SEPARATION ON CELLULOSE TRIBENZOATE AS STATIONARY PHASE

Materials and methods

A further unique field of application for cellulose derivatives was opened with the discovery of the utilization of special cellulose derivatives as stationary phase in chromatography for separating enantiomeric compounds. Derivatization of microcrystalline cellulose in a heterogeneous manner with preservation of the original parallel packing arrangement of native cellulose proved to be an excellent chiral recognition agent for separating enantiomeric compounds. First, Hesse and Hagel [16] received excellent separation applying cellulose triacetate (CTA I); later, Mannschreck et al. [17–19] added cellulose tribenzoate (CTBe I) and Riehl [15] introduced several at various positions at the phenyl ring-substituted cellulose triphenylcarbamate. Okamoto et al. [20] used surface-covered silica gels with a variety of cellulose and amylose derivatives as separation agent with great success.

High-resolution liquid chromatography columns packed with heterogeneously derivatized cellulose derivatives serve as a basic unit in an apparatus equipped with an UV- or OR- (optical rotatory) detector to differentiate between the optical antipodes. The resolution of the apparatus depends on the kind of cellulose derivative, the enantiomeric compound, and the eluent.

Results and discussion

Figure 9 illustrates the excellent chromatographic separation of Troeger's base, the compound shown by a space-filling model (left), and the UV-detection diagram by microcrystalline cellulose tribenzoate as separation agent. From the derivatization procedure of the microcrystalline cellulose, it was concluded that the separation process was predominantly occurring on materials consisting of parallel-arranged cellulosic molecules. Structural investigations on heterogeneously derivatized CTA I fibers led by a conformation and packing analysis based on X-ray fiber data [28,29] to parallel packing arrangement of the chains. A further investigation by minimization of the energy of crystal packing, discriminating between parallel vs. antiparallel arrangement [30], favors a parallel-packed two-chain unit cell. An extensive experimental study later came to a parallel-packed one-chain unit cell [29].

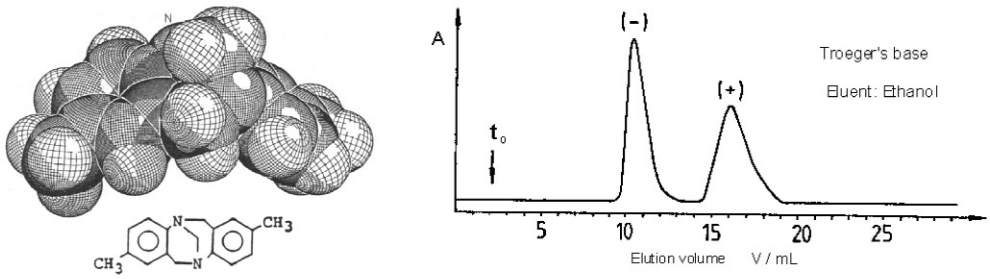

Fig. 9 Chromatographic separation (UV detection, right) of Troeger's base, which is represented by a space-filling model (left) on CTBe. Eluent: ethanol.

Only CTA I of poor crystallinity shows optimal resolving power for the enantiomeric separation. The interactions with the small molecules occur at the surface of the cellulosic crystallites or domains. An investigation of heterogeneously derivatized CTBe I, which exhibits excellent separation as shown in Fig. 9, confirms the parallel packing arrangement [15,31]. Amazingly, this kind of parallel packing was also found for homogeneously derivatized CTBe II, which was obtained by casting a film from the dissolved compound by evaporation of the solvent. Stretching this film, the X-ray fiber pattern of Fig. 10 was observed. Both patterns, CTBe I and CTBe II, can be indexed with the same one-chain unit cell and exhibit the same structure, a left-handed threefold helix, which is shown in Fig. 11. This study raises the question: What causes the different kind of packing arrangement, parallel and antiparallel. It is known that the antiparallel packing commonly occurs for crystals grown from solution.

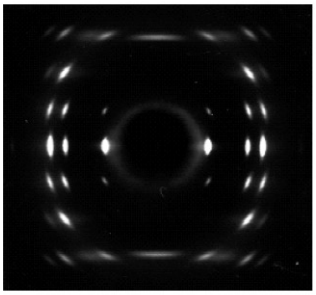

Fig. 10 Fiber X-ray pattern of an oriented film of CTBe II. A third-order meridional reflection indicates a threefold helix.

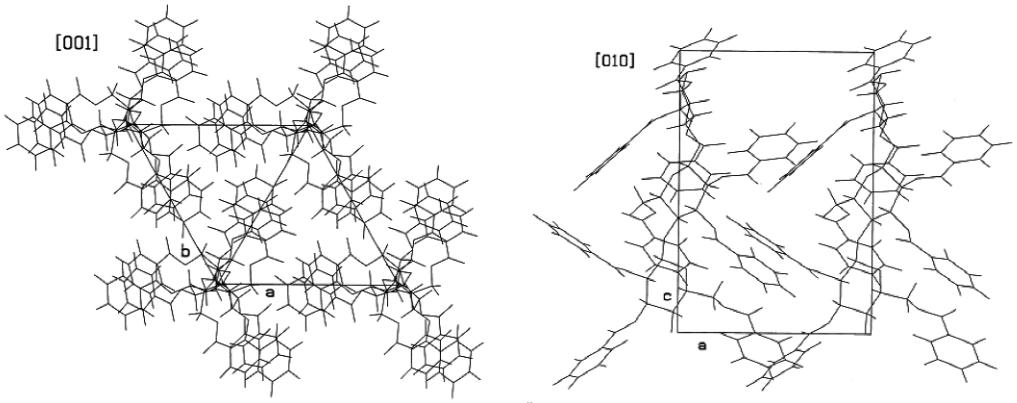

Fig. 11 Schematic representation of the parallel packing arrangement of a left-handed threefold CTBe helix within the one-chain trigonal unit cell projected down the chain axes (left) and a projection of the two corner chains along the *b*-axis (right).

A theoretical study was undertaken concerning the kind of packing arrangement, parallel and antiparallel, and concerning the influence on the size of crystallites or domains in cellulosic fibers [15]. The base plane of trigonal packed CTBe I was enlarged to serve as a model of a fiber with a large number of elementary units (fixed trigonal grid). This kind of grid facilitates calculations of the distances between chains. The only physical property to be considered in this study was an average interaction caused by the polarity of chains in a down and up direction with respect to the base plane. The theoretically introduced ratio of strength of the interactions between the chains varies from preferring an all parallel to an all antiparallel model.

A probability parameter r related to the ratio of the strength of interaction was introduced to describe the chain directions on the two-dimensional lattice: $r = 1$ is chosen for a parallel running chain with regard to a given chain, $r = 0$ for an antiparallel running one, and $0 < r < 1$ for statistical packing with increasing preference for parallel packing with growing r value. The overall parameter r is determined by considering the interaction energy of a chain with the surrounding ones. The number of adjacent parallel running chains in up or down direction represents a criterion for the extension of a domain. An illustration of the statistically distributed chains on the large base plane (fiber) is shown in Fig. 12a–e for selected parameters r. Such patterns can be calculated starting from various nuclei, e.g., beginning from the center or from one of the brims as realized in the illustrations. In the antiparallel arrangement of Fig. 12a with $r = 0$, the domain size is represented by the cross-section of a single chain, which is about 12 Å for CTBe. Large numbers of parallel chains (ca. 170 Å as average cross-section for CTBe) are observed for a parameter $r = 0.85$ (Fig. 12e) in up direction and the same amount of chains in down direction. The statistically arranged areas with parallel chains are decreasing for decreasing parameter r. For $r = 0.60$, the average cross-section of parallel chains amounts to 34 Å for CTBe, which leads to an increase of the total surface as compared to Fig. 12e considering all the domains (crystallites). Besides the interaction between chains, a further parameter, the disorder and defects, influences the size of the crystallite. A large disorder within the crystallites causes small domain sizes. The origin of the actual disorder within the crystallites of CTBe is not known.

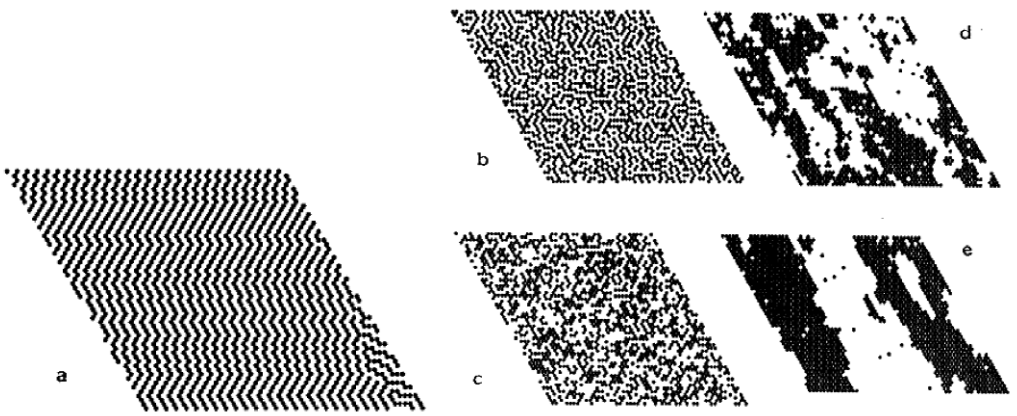

Fig. 12 Model of chain packing within a fiber with various ratios of interaction parameters r between chains of different polarity. ●: up chains, white dots (areas): down chains. (a) $r = 0$, (b) $r = 0.25$, (c) $r = 0.5$, (d) $r = 0.75$, (e) $r = 0.85$.

The packing arrangement of the fiber model in Fig. 12e exhibits large areas consisting of parallel running molecules, half of them pointing in up and half of them pointing in down direction. Such a model was discussed as prerequisite for parallel-packed chains in native cellulose I, which can be converted to antiparallel running chains of cellulose II by the mercerization process. If we assume changes in chain interactions during the mercerization treatment, a conversion of chain polarity may occur by an inter-diffusion process and a similar antiparallel model may result as presented in Fig. 12a.

The theoretical model of chain polarities proposed can only be regarded as a first approximation, since it does not include three-dimensional packing interactions of chains nor can the r parameter be correlated to the disorder of the crystalline structure, which determines the actual size of the domains. Small domain sizes of parallel-packed chains possess large crystallite surfaces, which are a necessity to act as the recognition sites for enantiomeric compounds.

OUTLOOK

Science and technology moves toward the use of renewable materials and sustainable resources, of which cellulose plays a major role. Great progress has been achieved in recent years in cellulosic materials, especially in bacterial cellulose as a model compound and high-performance materials, of which the biotechnological synthesis of blood vessels represents one example [32].

At present, a great challenge of basic research is to mimic certain composites and structure of solids formed by nature, which have been created to serve special purposes as, e.g., the wood of trees. All these natural materials are sustainable. It is interesting that nature is able to form large bulk materials with cellulose, which are not solvable in common solvents and consist of resistant and durable structures. A few materials, some of them not well researched, are illustrated in Fig. 13. They may be regarded as model composites as well as a design of materials to be achieved in the future. The stem (rod) of the palm tree leaf joins the main trunk of the tree as a planar laminate. It is amazing that this construction of the leaf of a palm tree starting from a two-dimensional laminate going over to a three-dimensional bulk materials, is strong enough to withstand the heavy winds of a typhoon or hurricane.

Almost unbreakable cactus thorns serve the Indians of South America as nails. However, compounds in the thorns might be washed out, and a breakable material like wood is obtained.

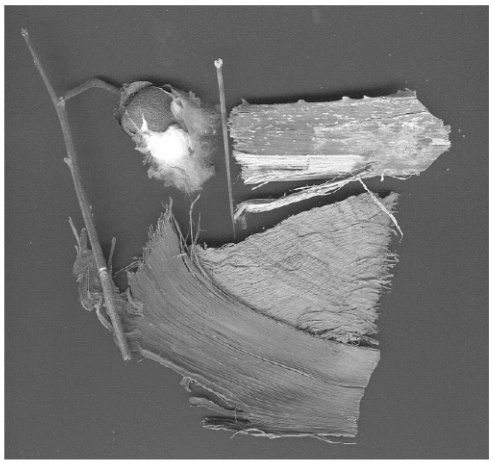

Fig. 13 Diversity of cellulose materials produced by nature to serve certain purposes. Left: a cotton ball with fine linters to transport seeds. Right (upper and lower part): Part of a palm tree leaf. Upper part: Bundles of fibers are glued together to form the rod-like stem of the leaf. Lower part: The two-dimensional section of the leaf joining the trunk of the tree. The fibers are running in almost perpendicular direction in the two layers shown and glued to form a strong laminate. Upper middle: A cactus thorn representing oriented and almost unbreakable cellulose composite materials.

REFERENCES

1. K. Hess. *Die Chemie der Zellulose und Ihrer Begleiter*, Akad. Verlagsges., Leipzig (1928).
2. D. N.-S. Hon. In *Emerging Technologies for Materials and Chemicals from Biomass*, ACS Symposium Series 476, R. M. Rowell, T. P. Schultz, R. Narayan (Eds.), American Chemical Society, Washington, DC (1992).
3. *Ullmann's Encyclopedia of Industrial Chemistry*, Vol. A5, VCH, Weinheim (1986).
4. R. Dönges. *Das Papier* **12**, 653 (1997).
5. F. Müller, Ch. Leuschke. In *Kunststoffhandbuch. Vol. 3/1: Technische Thermoplaste*, G. W. Becker, D. Braun (Eds.), pp. 396-457, Hanser, München (1992).

6. M. Marx-Figini. *J. Polym. Sci. C* **28**, 57 (1969).
7. A. Amash, P. Zugenmaier. *Polym. Bull.* **40**, 251 (1998).
8. A. Amash, P. Zugenmaier. *Polymer* **41**, 1589 (2000).
9. A. Amash, F.-I. Hildebrandt, P. Zugenmaier. *Design. Monom. Polym.* **5**, 385 (2002).
10. A. Amash. Doctoral thesis, TU Clausthal, Clausthal-Zellerfeld (1997).
11 P. Weigel, J. Ganster, H.-P. Fink, J. Gassan, K. Uihlin. *Kunststoffe-Plast. Europe* **92**, 95 (2002).
12. A. K. Bledzki, H.-P. Fink, K. Specht. *J. Appl. Sci.* **93**, 2150 (2004).
13. C. M. Clemons, A. J. Giacomin, D. F. Caulfield. *Antec* 1432 (1998).
14. F.-I. Hildebrandt. Doctoral thesis, TU Clausthal, Clausthal-Zellerfeld (1999).
15. K. Riehl. Doctoral thesis, TU Clausthal, Clausthal-Zellerfeld (1992).
16. (a) G. Hesse, R. Hagel. *Chromatographia* **6**, 277 (1973); (b) G. Hesse, R. Hagel. *Chromatographia* **9**, 62 (1976).
17. H. Koller, K.-H. Rimböck, A. Mannschreck. *J. Chromatogr.* **282**, 89 (1983).
18. (a) K.-H. Rimböck, F. Kastner, A. Mannschreck. *J. Chromatogr.* **329**, 307 (1985); (b) K.-H. Rimböck, F. Kastner, A. Mannschreck. *J. Chromatogr.* **351**, 346 (1986).
19. K.-H. Rimböck, M.-A. Cuyegkeng, A. Mannschreck. *Chromatographia* **21**, 223 (1986).
20. Y. Okamoto, E. Yashima. *Angew. Chem., Int. Ed.* **37**, 1021 (1998).
21. T. Karstens, J. Schätzle, R. Kohler, M. Wedler, M. Tubach. U.S. Patent 5883025 (1999).
22. A. Amash, P. Zugenmaier. *J. Appl. Polym. Sci.* **63**, 1143 (1997).
23. A. Amash, P. Zugenmaier. *J. Polym. Sci. B: Polym. Phys.* **35**, 1439 (1997).
24. J. Smook, A. J. Pennings. *Colloid Polym. Sci.* **262**, 712 (1984).
25. K. Schmidt. Doctoral thesis, TU Clausthal, Clausthal-Zellerfeld (1999).
26. M. M. Colemann, C. J. Serman, D. E. Bhagwagar, P. C. Painter. *Polymer* **31**, 1187 (1990).
27. K. J. Edgar, T. J. Pecorini, W. G. Glasser. In *Cellulose Derivatives*, ACS Symposium Series 688, T. Heinze, W. G. Glasser (Eds.), pp. 38–60, American Chemical Society, Washington, DC (1998).
28. A. Stipanovic, A. Sarko. *Polymer* **19**, 3 (1978).
29. P. Sikorski, M. Wada, L. Heux, H. Shintani, B. Stokke. *Macromolecules* **37**, 4547 (2004).
30. R. M. Wolf, E. Francotte, L. Glasser, I. Simon, H. A. Scheraga. *Macromolecules* **25**, 709 (1992).
31. P. Zugenmaier. In *Cellulose and Cellulose Derivatives*, J. F. Kennedy, G. O. Phillips, P. O. Williams, L. Piculell (Eds.), pp. 381–400, Woohead Publishing, Cambridge (1995).
32. D. Klemm, B. Heublein, H.-P. Fink, A. Bohn. *Angew. Chem., Int. Ed.* **44**, 3358 (2005).